

# Manual Labelling Artificially Inflates Deep Learning-Based Segmentation Performance on RGB Images of Closed Canopy: Validation Using TLS

M.J. Allen<sup>a</sup>, H.J.F Owen<sup>a</sup>, S.W.D. Grieve<sup>b,c</sup>, E.R. Lines<sup>a</sup>

<sup>a</sup>*Department of Geography, University of Cambridge, Cambridge, CB2 3EN, UK*

<sup>b</sup>*School of Geography, Queen Mary University of London, London, E1 4NS, UK*

<sup>c</sup>*Digital Environment Research Institute, Queen Mary University of London, , London, E1 1HH, UK*

---

## Abstract

Monitoring forest dynamics at an individual tree scale is essential for accurately assessing ecosystem responses to climate change, yet traditional methods relying on field-based forest inventories are labor-intensive and limited in spatial coverage. Advances in remote sensing using drone-acquired RGB imagery combined with deep learning models have promised precise individual tree crown (ITC) segmentation; however, existing methods are frequently validated against human-annotated images, lacking rigorous independent ground truth. In this study, we generate high-fidelity validation labels from co-located Terrestrial Laser Scanning (TLS) data for drone imagery of mixed unmanaged boreal and Mediterranean forests. We evaluate the performance of two widely used deep learning ITC segmentation models - DeepForest (RetinaNet) and Detectree2 (Mask R-CNN) - on these data, and compare to performance on further Mediterranean forest data labelled manually. When validated against TLS-derived ground truth from Mediterranean forests, model performance decreased significantly compared to assessment based on hand-labelled from an ecologically similar site (AP50: 0.094 vs. 0.670). Restricting evaluation to only canopy trees shrank this gap considerably (Canopy AP50: 0.365), although performance was still far lower than on similar hand-labelled data. Models also performed poorly on boreal forest data (AP50: 0.142), although again increasing when evaluated on canopy trees only (Canopy AP50: 0.308). Both models showed very poor localisation accuracy at stricter IoU thresholds, even when restricted to canopy trees (Max AP75: 0.051). Similar results have been observed in studies using aerial LiDAR data, suggesting fundamental limitations in aerial-based segmentation approaches in closed canopy forests.

*Keywords:* Deep Learning, Terrestrial Laser Scanning, Forests, Instance Segmentation, Object Detection

---

## 1. Introduction

Accurately monitoring the current and changing state of forests is essential to predicting the impact of climate change on both forest dynamics, and the ecosystem services they provide. Historically, monitoring efforts have relied on field-based forest inventories which capture forest dynamics at the individual tree level (Fréjaville et al., 2019). This granularity is vital because the size, age and species of individuals, as well individual interactions, determine how both trees and whole forests respond to climate-induced stressors (Chen et al., 2022; Coomes et al., 2014; Fernández-de-Uña et al., 2023; Teskey et al., 2014). Yet, the labor-intensive nature of these methods poses significant challenges, limiting their scope and effectiveness in covering expansive (Scott and Gove, 2002) or inaccessible forest areas (Zeng et al., 2015). In contrast, satellite-based approaches offer a more scalable solution, but are limited by spatial resolution, often resulting in findings based on large-scale spectral averages rather than individual tree data - such as approaches using data from the Sentinel (Allen et al., 2024a; Lastovicka et al., 2020) or Landsat (Zhang et al., 2021) satellite constellations.

The increased availability of lower-cost and accessible airborne imagery from airplanes and drones (Ouaknine et al., 2023; Troles et al., 2024) combined with deep learning has revolutionized remote sensing-based forest monitoring by enabling large-scale, high-resolution observations of individual trees (Allen et al., 2024b; Karthigesu et al., 2024). Often, a component of these approaches is the detection and delineation of canopy tree crowns in aerial imagery, for example to assess tree size distribution (crucial to understand forest carbon sequestration; Stephenson et al. (2014)) or canopy health (Allen et al., 2024b; Şandric et al., 2022). Recent years have seen a surge in studies using deep learning to precisely delineate individual trees from airborne imagery (Allen et al., 2024b; Ball et al., 2023; Hao et al., 2021; Şandric et al., 2022; Sani-Mohammed et al., 2022; Weinstein et al., 2019), showcasing the potential for significant advancements in forest monitoring. However, a common theme among these studies is the lack of verification using independent ground truth data (Hao et al., 2021; Lines et al., 2022; Şandric et al., 2022; Yang et al., 2022), instead typically relying on crown delineations created by hand from visual assessment of aerial images to create test, train and validation datasets. This introduces unquantified uncertainty into downstream tasks using individually segmented imagery. Rigorous testing of methods using independent data are crucial for reliable deployment. Recent work on the reliability of tree segmentation from aerial LiDAR data has shown it may be inaccurate for segmenting all but the tallest canopy crowns (Cao et al., 2023), demonstrating the limitations of three dimensional data; and highlighting the need for independent ground-truthed testing of two-dimensional crown delineation

approaches.

Segmentation of individual trees from imagery is a very active research area. Early efforts, such as Onishi and Ise (2021), showed some accuracy applying non-machine learning (ML) methods to RGB data. More recently, deep learning-based developments have dominated (Diez et al., 2021), with studies relying on manually delineated data for test, train and validation. A seminal work in this area, DeepForest (Weinstein et al., 2019), applied a single-stage object detector (bounding box delineation), RetinaNet (Lin et al., 2018), pretrained on labels derived from aerial LiDAR and finetuned on hand-drawn labels of Californian forests, achieving precision and recalls of 0.69 and 0.61 respectively. Subsequent studies have applied instance segmentation, delineating non-rectangular crown polygons from imagery. Such methods often internally identify individual trees as bounding boxes, and then delineate crowns within these boxes. Mask R-CNN (He et al., 2017) is a popular architecture for crown delineation, often evaluated considering predictions with an intersection-over-union (IoU) of more than 0.5 as correct, and has been used, for example, to segment tropical forest canopies in French Guiana and Malaysia (Ball et al., 2023), plantations in China (Hao et al., 2021) and dead trees in Scotland (Chiang et al., 2020). Using an IoU threshold of 0.5, these studies report F1 scores of 0.64 (Ball et al., 2023) and 0.91 (Hao et al., 2021), and a mean-average-precision of 0.54 (Chiang et al., 2020) respectively, with all studies relying on manually labelled data.

Beyond Mask R-CNN, other deep learning-based instance segmentation models have shown promise on manually labelled data. Ji et al. (2024) applied BlendMask (Chen et al., 2020) to high-resolution satellite data of low diversity forests near Beijing, achieving an F1-score of 0.86 at an IoU threshold of 0.5. Speckenwirth et al. (2024) investigated multiple instance segmentation models on multispectral aerial images of unmanaged forest in Germany, with their best model achieving an F1-score of 0.84. Li et al. (2023) developed a multitask network to produce tree counts and canopy maps from aerial data in Denmark at a national scale, although this approach did not delineate individual crowns. Pedley and Morgenroth (2025) combined DeepLabV3 (Chen et al., 2017) and SAM (Kirillov et al., 2023) for instance segmentation of urban trees in New Zealand, achieving an F1 score of 0.934 at an unspecified IoU threshold. Notably, the use of model composition - prompting SAM with semantic segmentation masks from DeepLabV3 - did not require individually segmented data for training, only evaluation.

The rise in deep learning approaches has been accompanied by a rise in initiatives providing open access crown instance segmentation data from aerial imagery. Five such data initiatives are listed in Table 1. BAMFORESTS (Troles et al., 2024)

Table 1: Comparison of Aerial Crown Instance Segmentation Datasets.

Dataset	Location	Area (ha)	Resolution	Crowns
<b>BAMFORESTS</b> <sup>1</sup>	Bavaria, Germany	105	1.7 cm	27,160
Cloutier et al.	Quebec, Canada	44	2 cm	22,933
<b>SiDroForest</b> <sup>2</sup>	Siberia	–	3 cm	20,214*
Jansen et al.	N. Australia	7	2 cm	2,547
<b>OAM-TCD</b> <sup>3</sup>	Global	–	10 cm	336,000**

\*Includes 872 manually labeled and 19,342 automatically extracted crowns

\*\*Approximately 280,000 individual trees and 56,000 tree groups

Note: Area not specified for SiDroForest and OAM-TCD datasets

<sup>1</sup>Troles et al. (2024)

<sup>2</sup>van Geffen et al. (2022)

<sup>3</sup>Veitch-Michaelis et al. (2024)

manually delineated crowns using human experts, with a random subset verification through in-situ field visits. Cloutier et al. (2024) combined manual orthomosaic delineation with GNSS field surveys marking individual trunk locations, likely ensuring a high degree of accuracy in the total tree count. SiDroForest (van Geffen et al., 2022) contains two subsets: 872 manually validated crowns and 19,342 crowns automatically extracted using watershed segmentation on Structure-from-Motion (SfM) derived canopy height models. Point clouds derived from SfM are generally considered lower-fidelity than aerial LiDAR, which in turn may be inaccurate for segmenting all but the largest canopy crowns (Cao et al., 2023). Jansen et al. (2023) relied solely on manual delineation in ArcGIS using orthomosaic imagery, without additional validation steps. OAM-TCD (Veitch-Michaelis et al., 2024) employed a multi-stage approach where paid non-expert annotators performed initial delineation with model assistance, followed by an expert review of the resulting annotations. The annotation protocol conservatively instructed annotators to segment closed canopy only if individual trees could be unambiguously identified, otherwise labeling such areas as “closed canopy.”

Terrestrial Laser Scanning (TLS) data may offer rigorous independent data for aerial crown segmentation benchmarking when co-located with imagery. TLS data comprises point clouds taken using ground-based LiDAR sensors, which are able to capture forest structure at the millimetre to centimetre scale. Crucially, the

additional high resolution structural information present in these data enables highly accurate individual tree segmentation - even using automated methods - to accuracies of centimetres or better (Wielgosz et al., 2023, 2024; Wilkes et al., 2023; Xiang et al., 2023, 2024). This precision, which introduces spatial errors comparable to only a few pixels in aerial imagery, makes TLS-derived crown delineations an ideal ground truth reference.

In this work we generate instance segmentation labels for aerial imagery directly from co-located individually segmented TLS, an ultra high-fidelity ground-based LiDAR. By superimposing segmented trees from these data on orthoimagery, we generate high quality test data for evaluating two common methods. We answer the following questions:

1. How well do pretrained segmentation models perform on unmanaged forest canopies in Mediterranean and boreal forests, when validated against high-fidelity ground truth data from an independent instrument?
2. Does the measured performance differ to that on a similar ecosystem that has been labelled by hand?
3. Does performance vary according to tree height, as seen for aerial LiDAR?

## 2. Methods

### 2.1. Data

#### 2.1.1. Study Areas

We collected both TLS data and drone imagery from 15 plots in boreal forests in the **Joensuu** region of Eastern Finland in summer 2022, and 19 plots from Mediterranean forests in the **Alto Tajo** Natural Park in central Spain in summer 2021. These plots are in the FUNDIV exploratory forest plot network (Ratcliffe et al., 2017). Plots are unmanaged and contain both coniferous and deciduous trees, with up to three dominant canopy species in Finland (*Picea abies*, *Pinus sylvestris* and *Betula spp.*) and up to four in Spain (*Pinus nigra*, *P. sylvestris*, *Quercus ilex* and *Quercus faginea*). We collected drone imagery without TLS from nine plots in **Almorox** (Allen et al., 2024b; Moreno-Fernández et al., 2022), central Spain, in summer 2019, in plots dominated by *Pinus pinea*. Both Spanish datasets represent unmanaged Mediterranean forests with structure and diversity impacted by water limitation, while Finnish data represent mixed boreal forests. All data were collected during the growing season, with trees leaf-on in all plots. A breakdown of the number of crowns visible from the air in each plot is available in Appendix B. As drone flights covered larger areas than the field plots, we use the term ‘area’ to describe a region within a site covered by a single drone flight and corresponding orthomosaic, and the term ‘plot’ to describe the subset area where TLS data was collected.

#### 2.1.2. Data Acquisition & Processing

*TLS Point Clouds.* One plot of 30×30 m was located in each area of the Joensuu and Alto Tajo sites. Plots were scanned using a Riegl VZ 400i with a TLS pulse repetition rate of 600 kHz. Scan locations were spaced in a grid pattern with 10 m spacing, with both upright and horizontal scans in each scan position, and additional scans outside plot boundaries. Trees were individually segmented from the point cloud data using TLS2Trees (Wilkes et al., 2023), followed by extensive manual refinement in CloudCompare 2.13.

*Drone Imagery.* Drone flights for all sites and area were conducted using a DJI Mavic Mini drone. Data was gathered with all relevant permissions and location-specific regulations observed, including the use of rotor guards. Raw images of dimensions 4000×2250px were obtained from nadir and oblique (55° below horizontal; Nesbit and Hugenholtz (2019)) view directions, with 95% front and 80% side overlap, from flights between 10-20 m above top canopy height. Detailed information on individual areas can be seen in Appendix B. Orthomosaics were generated using Agisoft Metashape 2.1.1 without the use of ground control points, as when used we found that inaccurate





*Manual Labelling.* Visible portions of crowns in the orthomosaic data from the Almorox site were delineated by hand (see Allen et al. (2024b)) from the orthomosaic data. This was performed in QGIS 3.30.

## 2.2. Crown Segmentation using Deep Learning

### 2.2.1. Models

We applied two popular pretrained deep learning models to our data, DeepForest (Weinstein et al., 2019) and Detectree2 (Ball et al., 2023). The architecture of DeepForest is based on RetinaNet (Lin et al., 2018) and Detectree2 on Mask R-CNN (He et al., 2017). We chose not to retrain either model on our data for two reasons. Firstly - this is the most common use case for these tools, and leads to the most widely applicable conclusions. Secondly - as each plot did not cover an entire orthomosaic, the degree of false negative sampling (where trees are visible but not labelled outside plot boundaries) in the data from the sites with TLS data (Joensuu, Alto Tajo) is high, which complicates training. Evaluation is unaffected, as predictions were clipped to the extent of the TLS plots.

Data were downsampled such that input tiles were of compatible size with the pretrained weights of DeepForest ( $400 \times 400$  px) and Detectree2 ( $1000 \times 1000$  px).

### 2.2.2. Evaluation

Both models were evaluated on all three sites - two labelled using co-located TLS (Joensuu, Alto Tajo) and one labelled by hand (Almorox).

For both DeepForest and Detectree2 we gridsearched across tile size and a non-maximum suppression (NMS) IoU jointly to maximise performance. A relative overlap of 0.5 across tiles was used for both models. At each gridsearch point, we calculate AP50 and AP75. We also report the best F1-score across confidence thresholds at the gridsearch point with the best AP50.

For the gridsearch points for each model with the highest AP50, we provide a full set of precision recall curves, and also show precision-recall curves for canopy trees only. We define a canopy tree as one with a maximum height greater than or equal to 75% of the maximum height within the same plot. To calculate precision on canopy trees - which requires including false positive predictions over a certain height - we assign a height values to prediction when more than 50% of its area is covered by a ground truth label. Since the ground truth labels have (next-to) no overlap by design, it is only possible for one height to be assigned per-prediction. Predictions that could not be assigned a height were discarded for calculations on canopy trees.

Detailed results for gridsearches are included in Appendix A. To ensure comparability, we assess both models on bounding box performance only - although Detectree2 is capable of producing non-rectangular delineations.

### 3. Results

Performance metrics for both DeepForest (DF) and Detectree2 (DT) can be seen in Table 2. Detectree2 outperformed DeepForest on all metrics (AP50, AP75, F1) across all three sites with the sole exception of AP75 on the data from Joensuu (Finland) - although the scores for both models are likely too low (DeepForest: 0.005; Detectree2: 0.002) to be significant. Notably, the performance gap was significant (Detectree2: 0.375; DeepForest: 0.036) when assessed at a strict IoU threshold of 0.75 on the manually delineated data.

Both models showed significantly lower performance overall on the TLS-labelled sites (Joensuu, Alto Tajo) compared to the manually labelled data (Almorox), which showed good performance (Best AP50: 0.670, AP75: 0.375, F1: 0.674). AP50 shrank from 0.385 (DeepForest) and 0.670 (Detectree2) to 0.05 (DeepForest) and 0.094 (Detectree2) when labels were generated using TLS (Alto Tajo) rather than labelled by hand (Almorox) in similar ecosystems. AP75 similarly shrank from 0.036 (DeepForest) and 0.375 (Detectree2) to 0.002 (DeepForest) and 0.011 (Detectree2). Maximum F1 scores at an IoU threshold of 50 shrank from 0.523 (DeepForest) and 0.674 (Detectree2) to 0.196 (DeepForest) and 0.227 (Detectree2).

The performance difference between manual and TLS data was significantly smaller when only considering canopy trees, at an IoU threshold of 0.5. AP50, for example, rose from 0.05 to 0.161 for DeepForest and 0.094 to 0.365 for Detectree2 on the TLS-labelled data from Alto Tajo - although still significantly lower than on the manually labelled data from a similar ecosystem (Best AP50: 0.670). Performance was still poor on both ecosystems when evaluated against the TLS data with a strict IoU threshold of 0.75 (Best AP75; Joensuu: 0.011, Alto Tajo: 0.051), regardless of whether models were assessed on canopy or all trees.

Precision-recall curves for all sites, for both Deepforest and Detectree2, can be seen in Figure 1. Detectree2 (bottom row) outperformed Deepforest (top row) consistently. Both showed reasonable overall performance on manually labelled data (left column), although the detection ability of DeepForest dropped significantly when assessed at an IoU threshold of 0.75 (blue lines) versus 0.5 (red lines). Detectree2 showed good performance on the manually labelled data at both thresholds. Both models showed consistently higher performance on the TLS data for canopy (Deepforest/Detectree2 AP50 Alto Tajo: 0.161/0.365, Joensuu: 0.257/0.308) than overall (Deepforest/Detectree2 AP50 Alto Tajo: 0.094/0.050, Joensuu: 0.142/0.105), although neither showed good performance on canopy trees at an IoU threshold of 0.75 (Deepforest/Detectree2 AP75 Alto Tajo: 0.005/0.051, Joensuu: 0.011/0.004).

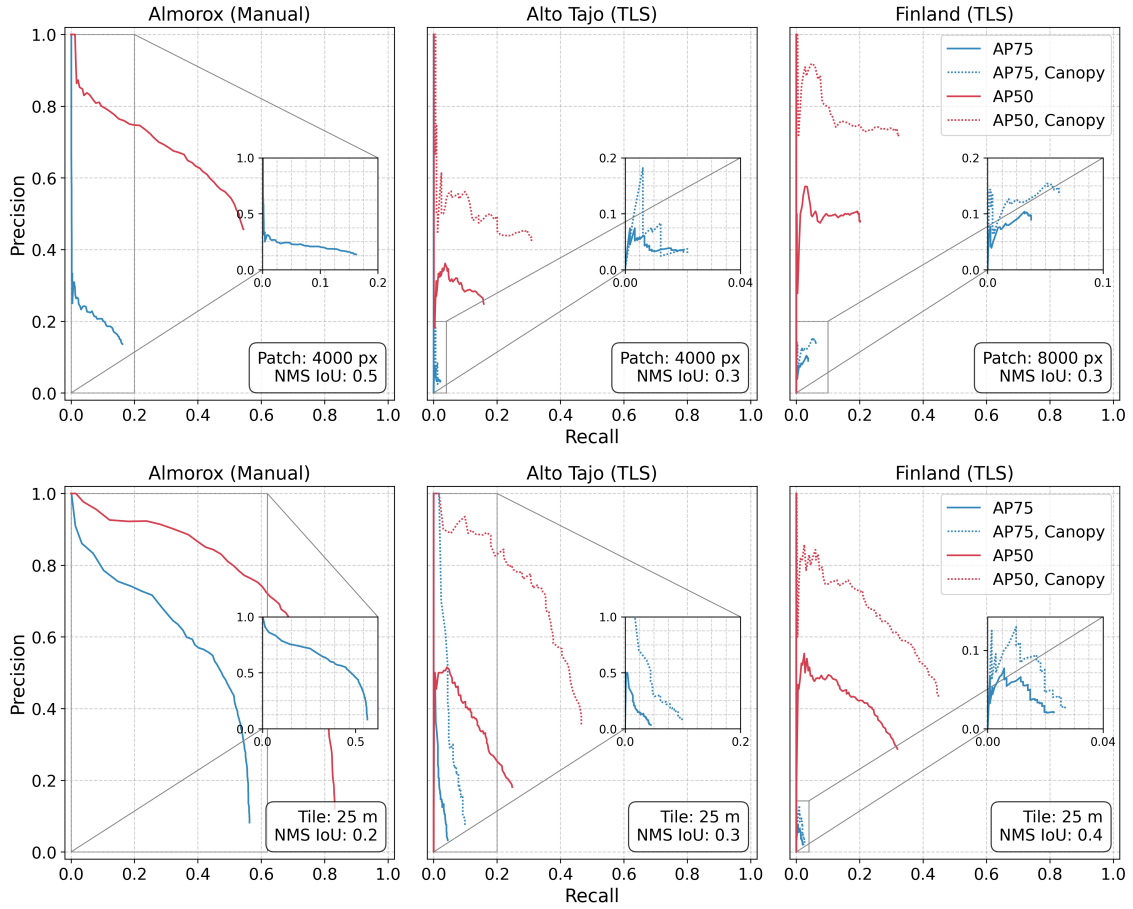


Figure 1: Precision-recall curves for **(top)** Deepforest and **(bottom)** Detectree2 at the best hyperparameters for each site. Performance was assessed at IoU thresholds of 0.5 (red lines) and 0.75 (blue lines). Precision-recall curves obtained when scoring against canopy trees only are shown using dashed lines for both IoU thresholds.

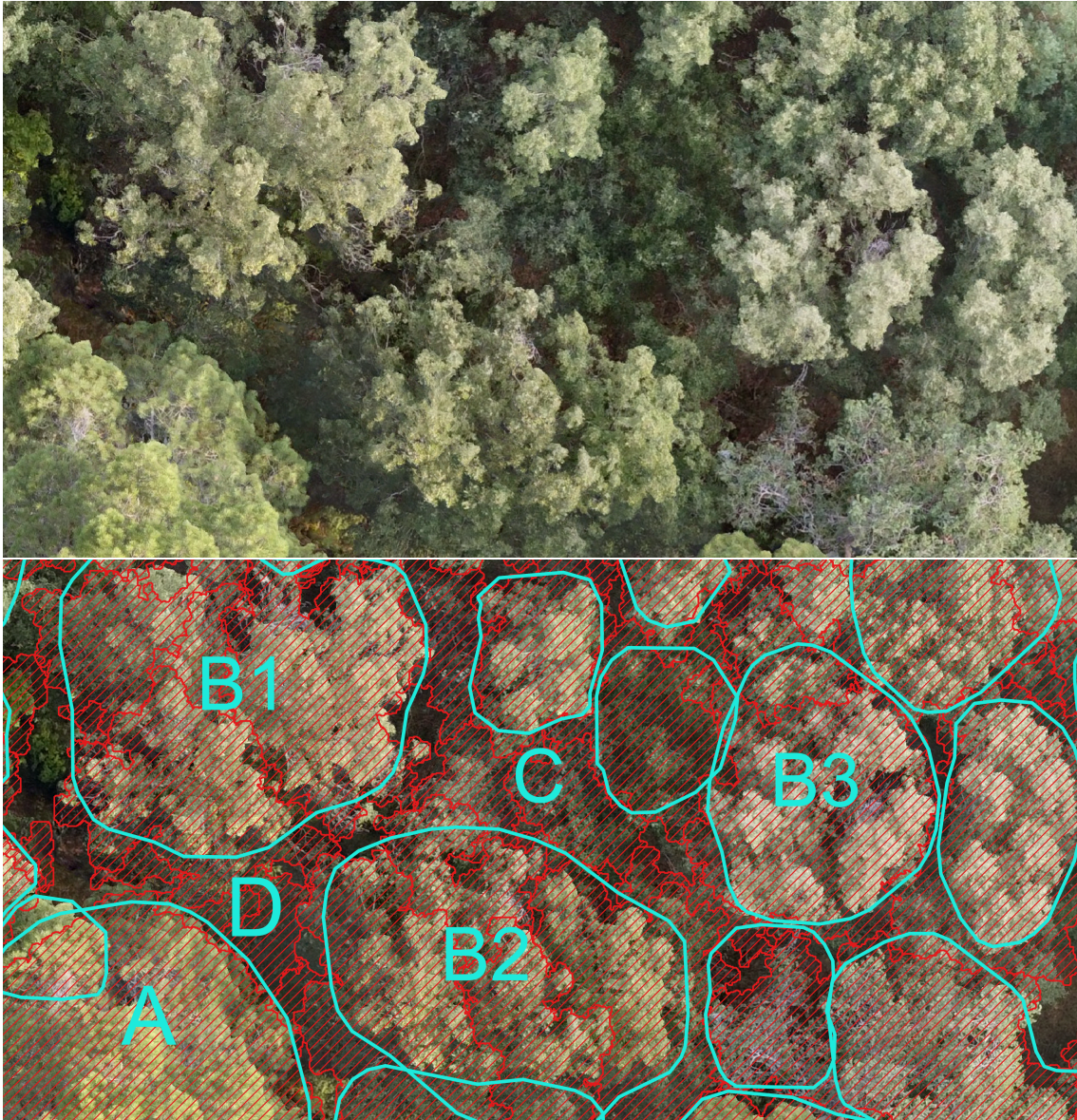


Figure 2: **(Top)** Image data with **(Bottom)** accompanying TLS-derived labels (Hashed, red) and Detectree2 predictions (Outlined, green) using the best hyperparameters. Several common sources of error are shown. **(A)** Large canopy tree segmented correctly. **(B1-3)** Canopy trees where the correct delineation is visually ambiguous - **(B1,2)** depict tightly grouped individual trees. **(B3)** is visually similar from above but is a single tree. **(C)** Sub-canopy trees that might be possible to predict but are generally omitted during hand-labelling. **(D)** Sub-canopy trees that are nominally visible from above but practically invisible due to shadowing or orthomosaic artefacting.

Table 2: Best parameters and corresponding metrics for **DeepForest (DF)** and **Detectree2 (DT)**. A relative overlap of 0.5 between tiles was used throughout. Canopy (Can) trees are  $\geq 75\%$  of the maximum height within each plot. NMS IoU refers to the minimum overlap for removal during post-processing, as opposed to the IoU correctness threshold used to calculate metrics. Reported F1-scores are maximised over confidence threshold, at an IoU threshold of 0.5.

Site	Mod	Tile Size	NMS IoU	AP <sub>50</sub>		AP <sub>75</sub>		F1	
				All	Can	All	Can	All	Can
Almorox (Manual)	DF	4000 px	0.5	0.385	–	0.036	–	0.523	–
	DT	25 m	0.2	0.670	–	0.375	–	0.674	–
Alto Tajo (TLS)	DF	4000 px	0.3	0.050	0.161	0.002	0.005	0.196	0.361
	DT	25 m	0.3	0.094	0.365	0.011	0.051	0.227	0.472
Joensuu (TLS)	DF	8000 px	0.3	0.105	0.257	0.005	0.011	0.284	0.445
	DT	25 m	0.4	0.142	0.308	0.002	0.004	0.311	0.458



Figure 3: Example of minor misalignment between TLS and image data. **(Left)** Raw imagery of a single tree. **(Middle)** Output polygon from Algorithm 1, with bounding box added for illustration. Ground truth polygons removed for surrounding trees to reduce visual clutter. Note cropping due to plot-edge effects. Predictions were also cropped to the extent of the plot after all other post-processing to eliminate the influence of plot-edge effects on evaluation. **(Right)**. Manually corrected polygon and bounding box (blue) overlaid on originals (red). The minor misalignment of individual branches causes a more pronounced shift in the full polygon than the bounding box. We evaluated segmentation using bounding boxes only.

## 4. Discussion

Our results show substantially lower performance for pretrained segmentation models on mixed unmanaged forest canopy when validated against high-fidelity ground truth data than previously reported in literature. Both study sites using TLS data showed poor AP50 values (0.105/0.142 and 0.050/0.094 for DeepForest/Detectree2 on Joensuu and Alto Tajo respectively; Table 2) and very poor AP75 scores (Joensuu: 0.005/0.002, Alto Tajo: 0.002/0.011). Even when maximising by adjusting confidence thresholds - which likely gives the best case scenario for model performance - the F1-scores were poor on both sites for both models (Joensuu: 0.284/0.311, Alto Tajo: 0.196/0.227). These metrics are markedly lower than those typically reported in crown delineation studies. Ball et al. (2023) reported an F1-score of 0.64 on tropical forest, Hao et al. (2021) reported a F1-score of 0.85 on plantation forest in China and Weinstein et al. (2019) reported an AP50 of 0.61 on open canopy forest in North America. Notably, all of these studies, along with others, report recalls almost exclusively higher than 0.5 (Ji et al., 2024; Šandric et al., 2022; Speckenwirth et al., 2024; Sun et al., 2023; Yang et al., 2022; Zhang et al., 2022), which was not achieved in any case on the TLS data (Figure 1). The performance of DeepForest was lower than that of Detectree2 throughout. This may stem from both differences in training data, with DeepForest being trained on open, single-story canopy data (temperate) and Detectree2 on closed canopy (albeit from a tropical ecosystem, unlike our evaluation data), or input resolution - with DeepForest using tiles of  $400 \times 400$  px and Detectree2  $1000 \times 1000$  px (internally - input tiles are downsampled to match these sizes). For the remainder of this section, we discuss results from Detectree2 only, although the lighter computational footprint of DeepForest could lend itself to large open canopy areas.

The performance disparity between TLS-validated and manually labeled sites from similar ecosystems was notable, with AP50 increasing from 0.094 to 0.670, AP75 from 0.011 to 0.375 and maximum F1 score from 0.227 to 0.674 on the manually labeled Almorox site, despite being ecologically similar to Alto Tajo. While very minor misalignment between TLS-derived labels and orthoimagery might affect performance metrics, our use of metrics based on bounding boxes rather than non-rectangular delineations should be permissive (Figure 3) enough to mitigate this effect.

The performance difference between canopy ( $\geq 75\%$  max plot height) and non-canopy trees offers some insight regarding this difference. Clear increases were observed for all metrics on both TLS sites (Joensuu: AP50 0.142  $\rightarrow$  0.308, AP75 0.002  $\rightarrow$  0.004, F1 0.311  $\rightarrow$  0.458; Alto Tajo: AP50 0.094  $\rightarrow$  0.365, AP75 0.011  $\rightarrow$  0.051, F1 0.311  $\rightarrow$  0.458). Notably, the range of precisions achieved in Figure 1

(bottom row) for canopy trees on the TLS data (right two columns, dashed lines) are similar to the precisions achieved on the manually labelled data, at least when using an IoU threshold of 0.5. Previous work reports similar results on aerial LiDAR data - with crown segmentation only accurate for canopy trees (Cao et al., 2023). Large canopy trees are visually obvious, and more likely to be included in manual training data as well as providing clear patterns for models to predict on.

Although the canopy precision is similar to the manually labeled data, the resulting average precision (AP50) is much lower because the recall is poorer. The phenomenon of poor detection rates in automated individual tree detection is often observed when using other aerial data sources such as LiDAR (Cao et al., 2023; Kaartinen et al., 2012), and our results on validating RGB-based segmentation appear to confirm this pattern. We offer two hypotheses as to why this is the case. Firstly, many sub-canopy trees are not labelled at all in manually delineated training data. Often, these trees are missed due to being barely visible due to either being small or in shadow (See Figure 2), even if they might theoretically be delineated from aerial images. Secondly - many trees are covered by labels, but incorrectly. Where there is significant intersection or overlap between crowns, visual separation is often ambiguous. We show an example of such a case in Figure 2 (B1-3). In Figure 1, it can be seen that even though the precisions at an IoU threshold of 0.5 are similar between the manual labels and canopy trees from TLS-labelled sites, the precisions are far poorer when using a stricter threshold of 0.75. This pattern is not observable in the manually labelled data, where performance is good at both thresholds. This huge drop in performance points to poor localisation ability - the models are able to detect the presence or absence of trees, but show little ability to separate crowns precisely in closed canopy. Manually labelled data suffers from a bias towards obvious canopy breaks - which do not necessarily correspond to individual trees (Figure 2 B1-B3). While it is possible that training models at significantly higher per-pixel resolutions and using advanced strategies to merge tiled predictions (Allen et al., 2024b) could solve this problem, it is not clear that the necessary structural information is observable from above. Decennially spaced benchmarking efforts for tree crown detection in aerial LiDAR data show only very small improvements in detection rates (Cao et al., 2023; Kaartinen et al., 2012), despite the explosion in machine learning-based methods over the same time frame - suggesting a fundamental challenge in detecting and delineating individual trees from aerial data, regardless of sensing technology. In some ecosystems, high species diversity can lead to higher variation in canopy reflectance, which might aid in crown separation (Ball et al., 2023), but our results suggest that RGB-based segmentation is unlikely to be robust in forests.

These limitations have particular relevance for national-scale forest inventory or



tree counting initiatives (Li et al., 2023; Sun et al., 2022). Individual tree mapping from RGB imagery alone may be infeasible in closed canopy forests, which are common in boreal, temperate and wet tropical ecosystems. While measurements of total canopy cover could be reliable, and crown delineation may be feasible in open canopy environments, attempts to count or delineate individual trees in closed canopy are likely to produce systematically inaccurate results. Given that similar observations have been made on segmentation using aerial LiDAR (Cao et al., 2023), this could be a fundamental limitation of the aerial perspective rather than a methodological shortcoming — the necessary structural-spectral information simply cannot be captured from above. We caution that the use of individual tree data from aerial imagery without ground validation may be unreliable, and that the approach adopted by OAM-TCD Veitch-Michaelis et al. (2024), with individual delineation only in open canopy, is more trustworthy in this case. Rapid national-scale forest inventories or other monitoring efforts seeking individual tree data may require alternative or complementary approaches to aerial sensing.

#### *Author Contributions*

**Conceptualisation:** All authors. **Data Curation:** M. J. Allen, E. R. Lines, H. J. F. Owen. **Formal Analysis:** M. J. Allen, S. W. D. Grieve, E. R. Lines. **Investigation:** M. J. Allen, E. R. Lines. **Visualisation:** M. J. Allen. **Writing - original draft:** M. J. Allen. **Writing - review and editing:** S. W. D. Grieve, E. R. Lines, H. J. F. Owen. **Supervision:** S. W. D. Grieve, E. R. Lines.

#### *Data & Code Availability*

Data and code are undergoing final preparations and will be made available through Zenodo and Github respectively prior to publication. Intermediate results such as model predictions will be provided in addition to raw data.

#### *Funding Sources*

M. J. Allen was supported by the UKRI Centre for Doctoral Training in Application of Artificial Intelligence to the study of Environmental Risks [EP/S022961/1]. E. R. Lines, S. W. D. Grieve and H. J. F. Owen were funded by a UKRI Future Leaders Fellowship awarded to E. R. Lines [MR/T019832/1].

## Appendix A. Gridsearch Results

Full results for the gridsearch outlined in Section 2.2.2 can be seen in Figure A.4 for DeepForest and Figure A.5 for Detectree2. Note that, for Detectree2 on Alto Tajo (Middle column, Figure A.5), the optimum tile size was 10 m despite our use of 25 m in the main text. This was not coincident with the optimum tile size for canopy trees, unlike both models on each of the other datasets. This is likely because some canopy trees will not fit within a single 10 m tile. We therefore chose to discard the results on 10 m tiles in the main text, and use 25 m tiles, which otherwise performed the best. Regardless, the overall performance of Detectree2 on the Alto Tajo data was near-constant when comparing 10 m to 25 m tiles (Figure A.5, middle column, top row) regardless, so the effect of this decision is likely insignificant.

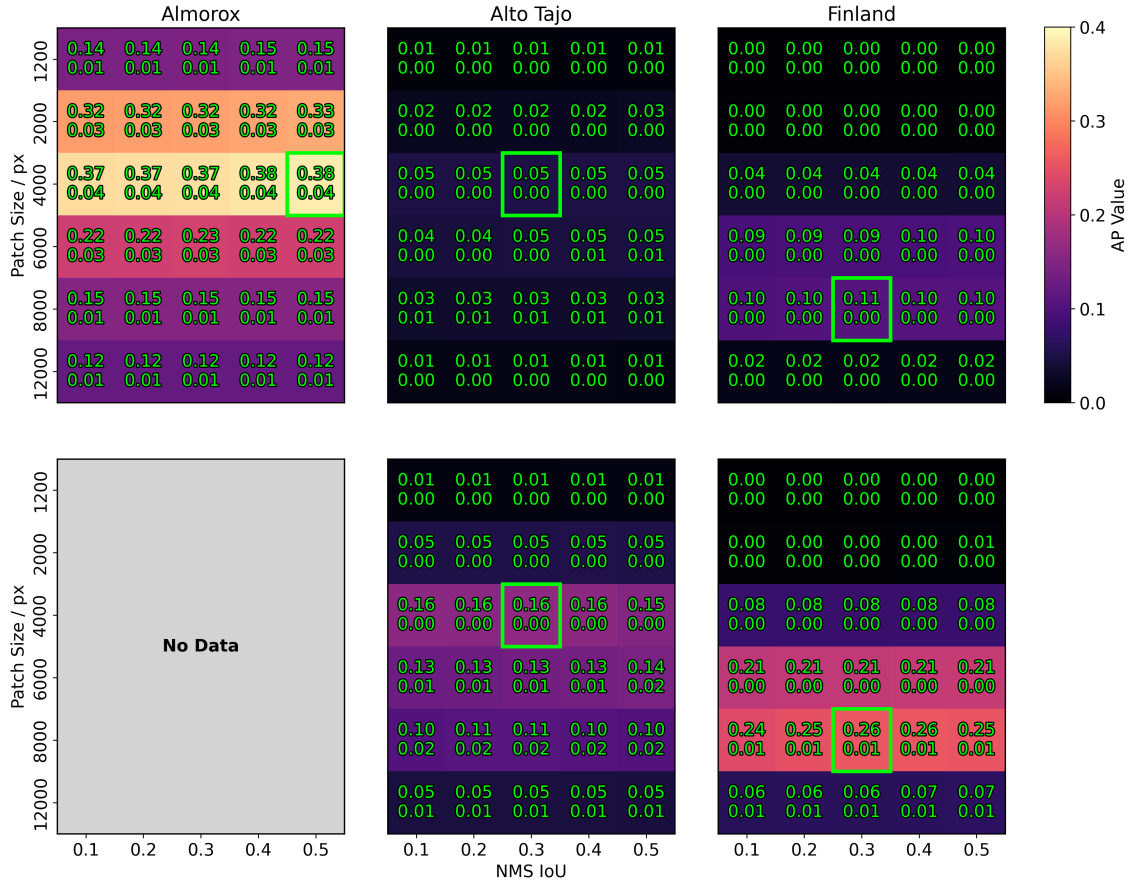


Figure A.4: Gridsearch results for **DeepForest** on Almorox (Manual labelling), Alto Tajo (TLS Labelling) and Joensuu (TLS Labelling). (**Top row**) Overall performance (**Bottom row**) Canopy performance. Top value within each cell denotes AP measured at an IoU of 0.5, and bottom values at 0.75. Cells coloured by AP50 for both overall and canopy, and best result outlined in green.

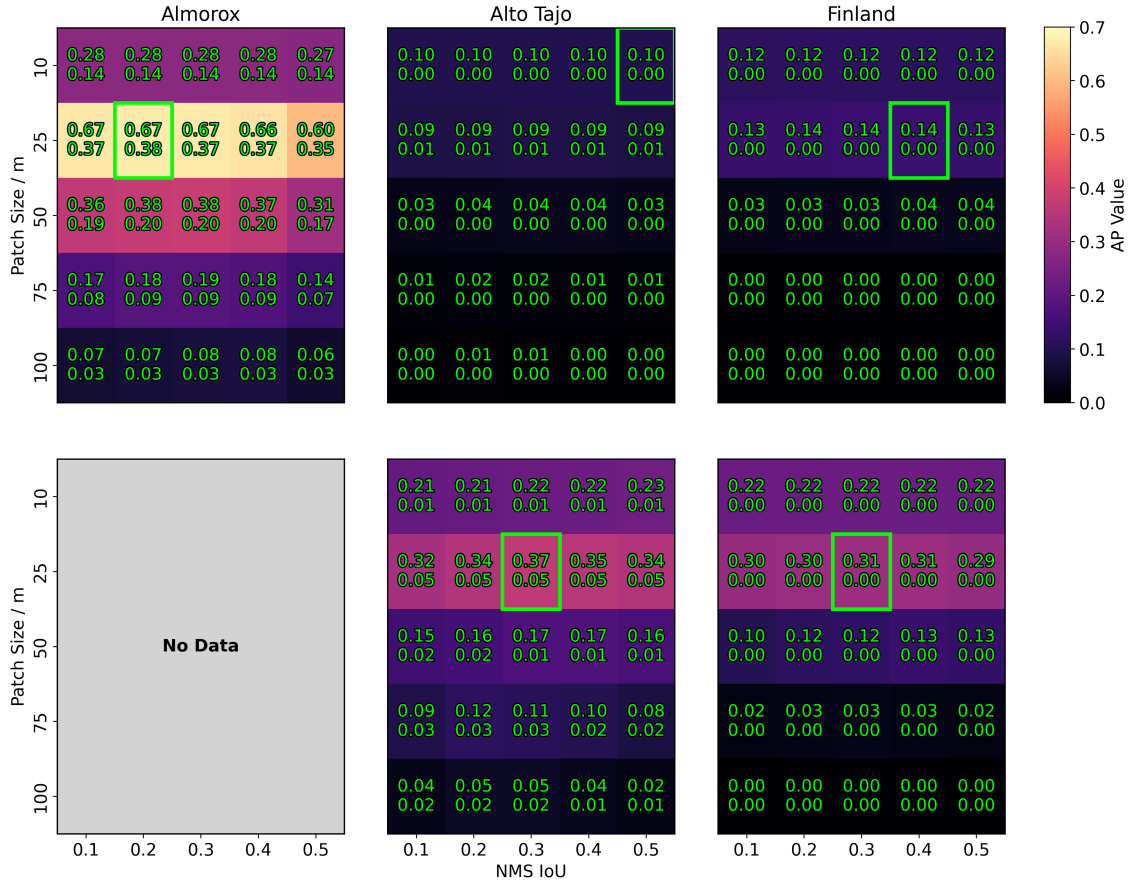


Figure A.5: Gridsearch results for **Detectree** on Almorox (Manual labelling), Alto Tajo (TLS Labelling) and Joensuu (TLS Labelling). (**Top row**) Overall performance. (**Bottom row**) Canopy performance. Top value within each cell denotes AP measured at an IoU of 0.5, and bottom values at 0.75. Cells coloured by AP50 for both overall and canopy, and best result outlined in green.

## Appendix B. Plot statistics

Site	Plot	Total Crowns	Max/Avg. Crown Area m <sup>2</sup>	Orthomosaic Dim. Px	GSD cmPx <sup>-1</sup>
Finland	FIN01	47	30.6 / 14.0	13893×19153	1.2
Finland	FIN02	59	28.8 / 11.1	14099×16256	1.2
Finland	FIN04	42	34.7 / 15.1	13495×19262	1.2
Finland	FIN09	123	27.0 / 7.5	12967×18781	1.1
Finland	FIN10	72	27.9 / 12.6	13683×20441	1.0
Finland	FIN12	141	29.7 / 5.2	14064×18253	1.2
Finland	FIN13	112	21.2 / 6.2	14007×16253	1.4
Finland	FIN15	90	25.6 / 8.6	11041×14511	1.4
Finland	FIN18	84	25.9 / 9.6	15928×18105	1.0
Finland	FIN19	67	25.3 / 12.2	15478×21625	1.0
Finland	FIN21	56	32.0 / 12.5	10118×13600	1.5
Finland	FIN23	101	16.9 / 7.8	12657×17100	1.3
Finland	FIN25	98	26.6 / 9.0	13260×18479	1.2
Finland	FIN27	78	20.0 / 8.5	13921×16942	1.2
Finland	FIN28	51	30.2 / 13.5	13767×17827	1.2
<b>Finland</b>	<b>Total/Avg.</b>	<b>1271</b>	<b>27.0 / 10.0</b>		<b>1.2</b>
Spain	SPA01	86	112.6 / 10.3	15815×14739	1.6
Spain	SPA02	39	24.1 / 10.4	13868×16802	1.5
Spain	SPA03	36	32.3 / 13.8	13240×16325	1.4
Spain	SPA05	61	116.8 / 10.8	16892×13702	1.3
Spain	SPA06	41	49.5 / 15.8	18162×21429	1.1
Spain	SPA13	79	48.2 / 7.3	14357×17166	1.5
Spain	SPA16	70	43.7 / 7.6	14481×15887	1.4
Spain	SPA17	125	40.5 / 7.4	18086×22048	1.2
Spain	SPA19	49	43.7 / 13.9	17561×14619	1.2
Spain	SPA23	35	36.3 / 9.8	13213×17005	1.4
Spain	SPA24	29	76.7 / 15.4	18613×16119	1.3
Spain	SPA25	51	58.1 / 13.7	14148×16868	1.2
Spain	SPA26	58	56.1 / 10.1	16343×16965	1.4
Spain	SPA27	22	61.2 / 16.3	17149×15086	1.3
Spain	SPA28	186	10.5 / 3.4	17314×13230	1.6
Spain	SPA29	121	85.7 / 6.7	16598×17239	1.3
Spain	SPA32	21	63.7 / 17.5	14276×17126	1.6
Spain	SPA35	41	43.6 / 9.3	16529×19296	1.7
Spain	SPA36	37	70.3 / 14.2	19592×17082	1.7
<b>Spain</b>	<b>Total/Avg.</b>	<b>1387</b>	<b>52.6 / 10.7</b>		<b>1.4</b>
<b>Combined</b>	<b>Total/Avg.</b>	<b>2658</b>	<b>40.3 / 10.4</b>		<b>1.3</b>

Table B.3: **Summary statistics** for the 34 areas, across the two TLS-labelled sites, in our data. One plot is found in each area and the plot name is used to reference both the area (the entire area covered by the drone imagery) and the plot (a subset of the area covered by drone imagery that was also covered by TLS data). A total of 2658 crowns were deemed to be visible from above using the TLS data and thus segmented within the images.

## Appendix C. Segmenting Orthomosaic Data Using TLS

### *Appendix C.1. Segmenting Orthoimagery using Point Clouds*

In this work, we undertook the task of segmenting tree crowns as-seen from above using TLS point clouds collected from the ground. We segmented visible crown area only, and therefore sought to remove overlap between crowns in our dataset, such that our data contained only areas of crown clearly visible in aerial imagery. Methods tested on our data were therefore evaluated on their ability to segment crowns that are visible from above, which is not the same as total crown area, nor does it include all trees in the TLS dataset, since sub-canopy trees will not be visible.

A simple approach to segment images might be to subtract crowns based on the maximum height of the respective tree. One advantage of this approach is that maximum height data is very often already available for existing crown segmentations. Such data could easily be processed into the desired form by simply assuming the crown of a taller tree is always above that of a shorter one, and subtracting the crown footprint of the taller from the smaller. This approach, however, does not consider height differences within crowns, which may result in part of the crown of a shorter tree lying above that of a taller one. We developed a pipeline applicable to point cloud data to determine the tree corresponding to the highest layer of the canopy at all points across an area of interest.

Our pipeline begins with the assumption that individual trees have been fully segmented from whole-plot TLS point clouds. At the time of writing, the pipeline should be applicable to individual point clouds of any format supported by the Point Data Abstraction Library (PDAL, Butler et al. (2024)). A Digital Surface Model (DSM) was first created for each of the individual tree point clouds using PDAL, with a DSM resolution of 2cm (a typical resolution for downsampled TLS data, or an orthomosaic) and gap filling using a window size of 1 pixel (2cm). It is possible for a DSM with disconnected nonzero regions to form, if any regions of the point cloud can be separated by a lateral gap of more than the DSM resolution plus the window size. These parameters were tuned to minimise this effect while maintaining high visual fidelity for the resulting segmentation. This selection was based on visual interpretation. Users may need to select different parameters under different drone flight protocols or with different instruments. A DSM resolution roughly equal to the orthomosaic resolution and a window size roughly equal to TLS resolution would be a reasonable starting point. The minimum and maximum  $x$  and  $y$  coordinates (`minx`, `miny`, `maxx`, `maxy`) encountered across all trees were recorded at this stage, and updated for each new tree processed, resulting in the minimum and maximum  $x$  and  $y$  coordinates for the entire plot after all trees are processed.

Next, an empty GDAL Virtual Dataset (VRT) was created, spanning the entire plot (`minx`, `miny`, `maxx`, `maxy`), at the same per-pixel resolution as the individual DSMs. We read this VRT as a `numpy` (Harris et al., 2020) array, `all_array`, to enable pixel-wise operations. This array was constructed with two bands - one corresponding to a DSM of the entire plot, and one where the pixel value is equal to the index of the tallest tree at that location. We iterated through the DSMs for each tree one at a time, aligning them with the VRT of the entire site, reading them as `numpy` arrays and then updating both channels of `all_array` using these individual arrays. After completing this loop, the layer containing the indices of the tallest tree at each pixel was polygonised using GDAL, resulting in a set of polygons where each polygon corresponds to a different tree. We then filtered these polygons, keeping only the largest polygon by area for each tree and removing any interior geometries.

This pipeline is shown as pseudocode in Algorithm 1.

## Appendix D. TLS-Orthomosaic Alignment

We made the following observations regarding generating orthomosaic data to align with TLS data that users may find useful should they need to apply this pipeline to new data.

- **Ground Control Point Accuracy:** Including GCPs measured with GNSS receivers in the field resulted in orthoimagery that did not align properly with TLS data. GCPs with lateral accuracy of 5-10 cm and vertical accuracy of 50-60 cm caused image misalignment during photogrammetric processing, leading to non-linear distortions in the orthomosaics. Since TLS data is precise at the level of individual branches, these distortions made alignment with orthomosaics impossible. Some software can adjust the alignment process based on GCP accuracy, which could help address these errors, although this in turn relies on accurate estimates of measurement uncertainty. Although Metashape 2.1.1 includes this functionality, we were unable to use it successfully despite having RMSE estimates for the GNSS coordinates. It is possible the RMSE estimates were also inaccurate. In contrast, generating orthoimagery without GCPs produced more accurate geometries, though the overall georeferencing accuracy was lower. In such cases, the entire image may be offset by several metres, but the geometries of individual crowns aligned better with the TLS point clouds. This type of error is straightforward to correct by hand using common GIS software, although potentially time consuming.
- **Photogrammetric Alignment:** Crown geometries were improved by not downsampling during alignment.



- **Ground Plane Accuracy:** Accurate estimation of ground plane orientation (z-axis direction) is critical for proper data alignment. Even small errors of  $3 - 4^\circ$  in the z-axis direction caused distortions in the orthoimagery - as the resulting view orientation will not be vertical - making alignment with TLS data impossible. These distortions may not be immediately obvious without directly comparing the two data sources. Inaccurate altitude estimates for GCPs can introduce this type of error regardless of lateral accuracy. The use of accurately located common targets (Maximum RMSE 1-2cm) or GCPs in both the drone imagery and TLS scans is likely the best approach to achieving strong alignment across the two data sources - noting that both their vertical and lateral accuracies must both meet this requirement.
- **Orthomosaic Artefacting:** Previous work constructing orthomosaic data of forests (Troles et al., 2024) for aerial segmentation reported small artefacts in the resulting images. We found that constructing a 3D model (corresponding to a surface type set to 'Arbitrary' in Metashape) from Depth Map data and then building the orthomosaics on the 3D model eliminated most of these artefacts compared to building orthomosaics on Digital Elevation Model (DEM) data.

## References

- Allen, M., Dorr, F., Gallego-Mejia, J.A., Martínez-Ferrer, L., Jungbluth, A., Kalaitzis, F., Ramos-Pollán, R., 2024a. Large Scale Masked Autoencoding for Reducing Label Requirements on SAR Data. doi:10.48550/arXiv.2310.00826, arXiv:2310.00826.
- Allen, M.J., Moreno-Fernández, D., Ruiz-Benito, P., Grieve, S.W.D., Lines, E.R., 2024b. Low-cost tree crown dieback estimation using deep learning-based segmentation. *Environmental Data Science* 3, e18. doi:10.1017/eds.2024.16.
- Ball, J.G.C., Hickman, S.H.M., Jackson, T.D., Koay, X.J., Hirst, J., Jay, W., Archer, M., Aubry-Kientz, M., Vincent, G., Coomes, D.A., 2023. Accurate delineation of individual tree crowns in tropical forests from aerial RGB imagery using Mask R-CNN. *Remote Sensing in Ecology and Conservation* 9, 641–655. doi:10.1002/rse2.332.
- Butler, H., Bell, A., Gerlek, M.P., chambbj, Gadomski, P., Manning, C., Loskot, M., Couwenberg, B., Barker, N., Ramsey, P., Dark, J., Chaulet, N., Rouault, E., Mann, K., Foster, C., Villemin, G., Rosen, M., Grigory, Moore, O., Lewis, S., McKelvey, K., Brookes, D., Evers, K., Dobias, M., Robert Coup, R., Vergara, V., xantares, Bram, Yonas, A., 2024. PDAL/PDAL: 2.7.1. Zenodo. doi:10.5281/ZENODO.10884408.
- Cao, Y., Ball, J.G.C., Coomes, D.A., Steinmeier, L., Knapp, N., Wilkes, P., Disney, M., Calders, K., Burt, A., Lin, Y., Jackson, T.D., 2023. Benchmarking airborne laser scanning tree segmentation algorithms in broadleaf forests shows high accuracy only for canopy trees. *International Journal of Applied Earth Observation and Geoinformation* 123, 103490. doi:10.1016/j.jag.2023.103490.
- Chen, H., Sun, K., Tian, Z., Shen, C., Huang, Y., Yan, Y., 2020. BlendMask: Top-Down Meets Bottom-Up for Instance Segmentation. doi:10.48550/arXiv.2001.00309, arXiv:2001.00309.
- Chen, L.C., Papandreou, G., Schroff, F., Adam, H., 2017. Rethinking Atrous Convolution for Semantic Image Segmentation. doi:10.48550/arXiv.1706.05587, arXiv:1706.05587.
- Chen, Z., Li, S., Wan, X., Liu, S., 2022. Strategies of tree species to adapt to drought from leaf stomatal regulation and stem embolism resistance to root properties. *Frontiers in Plant Science* 13, 926535. doi:10.3389/fpls.2022.926535.

- Chiang, C.Y., Barnes, C., Angelov, P., Jiang, R., 2020. Deep Learning-Based Automated Forest Health Diagnosis From Aerial Images. *IEEE Access* 8, 144064–144076. doi:10.1109/ACCESS.2020.3012417.
- Cloutier, M., Germain, M., Laliberté, E., 2024. Influence of temperate forest autumn leaf phenology on segmentation of tree species from UAV imagery using deep learning. *Remote Sensing of Environment* 311, 114283. doi:10.1016/j.rse.2024.114283.
- Coomes, D.A., Flores, O., Holdaway, R., Jucker, T., Lines, E.R., Vanderwel, M.C., 2014. Wood production response to climate change will depend critically on forest composition and structure. *Global Change Biology* 20, 3632–3645. doi:10.1111/gcb.12622.
- Diez, Y., Kentsch, S., Fukuda, M., Caceres, M.L.L., Moritake, K., Cabezas, M., 2021. Deep Learning in Forestry Using UAV-Acquired RGB Data: A Practical Review. *Remote Sensing* 13, 2837. doi:10.3390/rs13142837.
- Fernández-de-Uña, L., Martínez-Vilalta, J., Poyatos, R., Mencuccini, M., McDowell, N.G., 2023. The Role of Height-Driven Constraints and Compensations on Tree Vulnerability to Drought. *New Phytologist* 239, 2083–2098. doi:10.1111/nph.19130.
- Fréjaville, T., Fady, B., Kremer, A., Ducouso, A., Benito Garzón, M., 2019. Inferring phenotypic plasticity and population responses to climate across tree species ranges using forest inventory data. *Global Ecology and Biogeography* 28, 1259–1271. doi:10.1111/geb.12930.
- Hao, Z., Lin, L., Post, C.J., Mikhailova, E.A., Li, M., Chen, Y., Yu, K., Liu, J., 2021. Automated tree-crown and height detection in a young forest plantation using mask region-based convolutional neural network (Mask R-CNN). *ISPRS Journal of Photogrammetry and Remote Sensing* 178, 112–123. doi:10.1016/j.isprsjprs.2021.06.003.
- Harris, C.R., Millman, K.J., Van Der Walt, S.J., Gommers, R., Virtanen, P., Cournapeau, D., Wieser, E., Taylor, J., Berg, S., Smith, N.J., Kern, R., Picus, M., Hoyer, S., Van Kerkwijk, M.H., Brett, M., Haldane, A., Del Río, J.F., Wiebe, M., Peterson, P., Gérard-Marchant, P., Sheppard, K., Reddy, T., Weckesser, W., Abbasi, H., Gohlke, C., Oliphant, T.E., 2020. Array programming with NumPy. *Nature* 585, 357–362. doi:10.1038/s41586-020-2649-2.

- He, K., Gkioxari, G., Dollár, P., Girshick, R., 2017. Mask R-CNN. <https://arxiv.org/abs/1703.06870v3>.
- Jansen, A.J., Nicholson, J.D., Esparon, A., Whiteside, T., Welch, M., Tunstill, M., Paramjyothi, H., Gadhiraaju, V., van Bodegraven, S., Bartolo, R.E., 2023. Deep Learning with Northern Australian Savanna Tree Species: A Novel Dataset. *Data* 8, 44. doi:10.3390/data8020044.
- Ji, Z., Xu, J., Yan, L., Ma, J., Chen, B., Zhang, Y., Zhang, L., Wang, P., 2024. Satellite Remote Sensing Images of Crown Segmentation and Forest Inventory Based on BlendMask. *Forests* 15, 1320. doi:10.3390/f15081320.
- Kaartinen, H., Hyyppä, J., Yu, X., Vastaranta, M., Hyyppä, H., Kukko, A., Holopainen, M., Heipke, C., Hirschmugl, M., Morsdorf, F., Næsset, E., Pitkänen, J., Popescu, S., Solberg, S., Wolf, B.M., Wu, J.C., 2012. An International Comparison of Individual Tree Detection and Extraction Using Airborne Laser Scanning. *Remote Sensing* 4, 950–974. doi:10.3390/rs4040950.
- Karthigesu, J., Owari, T., Tsuyuki, S., Hiroshima, T., 2024. Improving the Estimation of Structural Parameters of a Mixed Conifer–Broadleaf Forest Using Structural, Textural, and Spectral Metrics Derived from Unmanned Aerial Vehicle Red Green Blue (RGB) Imagery. *Remote Sensing* 16, 1783. doi:10.3390/rs16101783.
- Kirillov, A., Mintun, E., Ravi, N., Mao, H., Rolland, C., Gustafson, L., Xiao, T., Whitehead, S., Berg, A.C., Lo, W.Y., Dollár, P., Girshick, R., 2023. Segment Anything. doi:10.48550/arXiv.2304.02643, arXiv:2304.02643.
- Lastovicka, J., Svec, P., Paluba, D., Kobliuk, N., Svoboda, J., Hladky, R., Stych, P., 2020. Sentinel-2 Data in an Evaluation of the Impact of the Disturbances on Forest Vegetation. *Remote Sensing* 12, 1914. doi:10.3390/rs12121914.
- Li, S., Brandt, M., Fensholt, R., Kariryaa, A., Igel, C., Gieseke, F., Nord-Larsen, T., Oehmcke, S., Carlsen, A.H., Junttila, S., Tong, X., d’Aspremont, A., Ciais, P., 2023. Deep learning enables image-based tree counting, crown segmentation, and height prediction at national scale. *PNAS Nexus* 2, pgad076. doi:10.1093/pnasnexus/pgad076.
- Lin, T.Y., Goyal, P., Girshick, R., He, K., Dollár, P., 2018. Focal Loss for Dense Object Detection. arXiv:1708.02002 [cs] arXiv:1708.02002.

- Lines, E.R., Allen, M., Cabo, C., Calders, K., Debus, A., Grieve, S.W.D., Miltiadou, M., Noach, A., Owen, H.J.F., Puliti, S., 2022. AI applications in forest monitoring need remote sensing benchmark datasets, in: 2022 IEEE International Conference on Big Data (Big Data), pp. 4528–4533. doi:10.1109/BigData55660.2022.10020772.
- Moreno-Fernández, D., Camarero, J.J., García, M., Lines, E.R., Sánchez-Dávila, J., Tijerín, J., Valeriano, C., Viana-Soto, A., Zavala, M.Á., Ruiz-Benito, P., 2022. The Interplay of the Tree and Stand-Level Processes Mediate Drought-Induced Forest Dieback: Evidence from Complementary Remote Sensing and Tree-Ring Approaches. *Ecosystems* 25, 1738–1753. doi:10.1007/s10021-022-00793-2.
- Nesbit, P.R., Hugenholtz, C.H., 2019. Enhancing UAV–SfM 3D Model Accuracy in High-Relief Landscapes by Incorporating Oblique Images. *Remote Sensing* 11, 239. doi:10.3390/rs11030239.
- Onishi, M., Ise, T., 2021. Explainable Identification and Mapping of Trees Using Uav Rgb Image and Deep Learning. *Scientific Reports* 11, 903. doi:10.1038/s41598-020-79653-9.
- Ouaknine, A., Kattenborn, T., Laliberté, E., Rolnick, D., 2023. OpenForest: A data catalogue for machine learning in forest monitoring. doi:10.48550/arXiv.2311.00277, arXiv:2311.00277.
- Pedley, D., Morgenroth, J., 2025. Detecting and measuring fine-scale urban tree canopy loss with deep learning and remote sensing. *ISPRS Open Journal of Photogrammetry and Remote Sensing* 15, 100082. doi:10.1016/j.ojphoto.2025.100082.
- Ratcliffe, S., Wirth, C., Jucker, T., van der Plas, F., Scherer-Lorenzen, M., Verheyen, K., Allan, E., Benavides, R., Bruelheide, H., Ohse, B., Paquette, A., Ampoorter, E., Bastias, C.C., Bauhus, J., Bonal, D., Bouriaud, O., Bussotti, F., Carnol, M., Castagnyrol, B., Češko, E., Dawud, S.M., Wandeler, H.D., Domisch, T., Finér, L., Fischer, M., Fotelli, M., Gessler, A., Granier, A., Grossiord, C., Guyot, V., Haase, J., Hättenschwiler, S., Jactel, H., Jaroszewicz, B., Joly, F.X., Kambach, S., Kolb, S., Koricheva, J., Liebersgesell, M., Milligan, H., Müller, S., Muys, B., Nguyen, D., Nock, C., Pollastrini, M., Purschke, O., Radoglou, K., Raulund-Rasmussen, K., Roger, F., Ruiz-Benito, P., Seidl, R., Selvi, F., Seiferling, I., Stenlid, J., Valladares, F., Vesterdal, L., Baeten, L., 2017. Biodiversity and ecosystem functioning relations in European forests depend on environmental context. *Ecology Letters* 20, 1414–1426. doi:10.1111/ele.12849.

- Şandric, I., Irimia, R., Petropoulos, G.P., Anand, A., Srivastava, P.K., Pleşoianu, A., Faraslis, I., Stateras, D., Kalivas, D., 2022. Tree's Detection & Health's Assessment from Ultra-High Resolution UAV Imagery and Deep Learning. *Geocarto International* 37, 10459–10479. doi:10.1080/10106049.2022.2036824.
- Sani-Mohammed, A., Yao, W., Heurich, M., 2022. Instance Segmentation of Standing Dead Trees in Dense Forest from Aerial Imagery Using Deep Learning. *ISPRS Open Journal of Photogrammetry and Remote Sensing* 6, 100024. doi:10.1016/j.ojphoto.2022.100024.
- Scott, C., Gove, J., 2002. Forest inventory, in: *Encyclopedia of Environmetrics*. John Wiley & Sons, Chichester:. volume 2, pp. 814–820.
- Speckenwirth, S., Brandmeier, M., Paczkowski, S., 2024. TreeSeg—A Toolbox for Fully Automated Tree Crown Segmentation Based on High-Resolution Multispectral UAV Data. *Remote Sensing* 16, 3660. doi:10.3390/rs16193660.
- Stephenson, N.L., Das, A.J., Condit, R., Russo, S.E., Baker, P.J., Beckman, N.G., Coomes, D.A., Lines, E.R., Morris, W.K., Rüger, N., Álvarez, E., Blundo, C., Bunyavejchewin, S., Chuyong, G., Davies, S.J., Duque, Á., Ewango, C.N., Flores, O., Franklin, J.F., Grau, H.R., Hao, Z., Harmon, M.E., Hubbell, S.P., Kenfack, D., Lin, Y., Makana, J.R., Malizia, A., Malizia, L.R., Pabst, R.J., Pongpattananurak, N., Su, S.H., Sun, I.F., Tan, S., Thomas, D., van Mantgem, P.J., Wang, X., Wiser, S.K., Zavala, M.A., 2014. Rate of tree carbon accumulation increases continuously with tree size. *Nature* 507, 90–93. doi:10.1038/nature12914.
- Sun, Y., Li, Z., He, H., Guo, L., Zhang, X., Xin, Q., 2022. Counting trees in a subtropical mega city using the instance segmentation method. *International Journal of Applied Earth Observation and Geoinformation* 106, 102662. doi:10.1016/j.jag.2021.102662.
- Sun, Z., Xue, B., Zhang, M., Schindler, J., 2023. YOLOv8E: An efficient YOLOv8 method for instance segmentation of individual tree crowns in Wellington City, New Zealand. *Journal of the Royal Society of New Zealand* 0, 1–26. doi:10.1080/03036758.2024.2424802.
- Teskey, R., Wertin, T., Bauweraerts, I., Ameye, M., Mcguire, M.A., Steppe, K., 2014. Responses of tree species to heat waves and extreme heat events. *Plant, Cell & Environment* 38, 1699–1712. doi:10.1111/pce.12417.

- Troles, J., Schmid, U., Fan, W., Tian, J., 2024. BAMFORESTS: Bamberg Benchmark Forest Dataset of Individual Tree Crowns in Very-High-Resolution UAV Images. *Remote Sensing* 16, 1935. doi:10.3390/rs16111935.
- van Geffen, F., Heim, B., Brieger, F., Geng, R., Shevtsova, I.A., Schulte, L., Stuenzi, S.M., Bernhardt, N., Troeva, E.I., Pestryakova, L.A., Zakharov, E.S., Pflug, B., Herzsuh, U., Kruse, S., 2022. SiDroForest: A comprehensive forest inventory of Siberian boreal forest investigations including drone-based point clouds, individually labeled trees, synthetically generated tree crowns, and Sentinel-2 labeled image patches. *Earth System Science Data* 14, 4967–4994. doi:10.5194/essd-14-4967-2022.
- Veitch-Michaelis, J., Cottam, A., Schweizer, D., Broadbent, E.N., Dao, D., Zhang, C., Zambrano, A.A., Max, S., 2024. OAM-TCD: A globally diverse dataset of high-resolution tree cover maps. doi:10.48550/arXiv.2407.11743, arXiv:2407.11743.
- Weinstein, B., Marconi, S., Bohlman, S., Zare, A., White, E., 2019. Individual Tree-Crown Detection in RGB Imagery Using Semi-Supervised Deep Learning Neural Networks. *Remote Sensing* 11, 1309. doi:10.3390/rs11111309.
- Wielgosz, M., Puliti, S., Wilkes, P., Astrup, R., 2023. Point2Tree (P2T)—Framework for parameter tuning of semantic and instance segmentation used with mobile laser scanning data in coniferous forest. *Remote Sensing* 15, 3737.
- Wielgosz, M., Puliti, S., Xiang, B., Schindler, K., Astrup, R., 2024. SegmentAnyTree: A sensor and platform agnostic deep learning model for tree segmentation using laser scanning data. *Remote Sensing of Environment* 313, 114367. doi:10.1016/j.rse.2024.114367.
- Wilkes, P., Disney, M., Armston, J., Bartholomeus, H., Bentley, L., Brede, B., Burt, A., Calders, K., Chavana-Bryant, C., Clewley, D., Duncanson, L., Forbes, B., Krisanski, S., Malhi, Y., Moffat, D., Origo, N., Shenkin, A., Yang, W., 2023. TLS2trees: A scalable tree segmentation pipeline for TLS data. *Methods in Ecology and Evolution* 14, 3083–3099. doi:10.1111/2041-210X.14233.
- Xiang, B., Peters, T., Kontogianni, T., Vetterli, F., Puliti, S., Astrup, R., Schindler, K., 2023. Towards accurate instance segmentation in large-scale LiDAR point clouds. doi:10.48550/arXiv.2307.02877, arXiv:2307.02877.

- Xiang, B., Wielgosz, M., Kontogianni, T., Peters, T., Puliti, S., Astrup, R., Schindler, K., 2024. Automated forest inventory: Analysis of high-density airborne LiDAR point clouds with 3D deep learning. *Remote Sensing of Environment* 305, 114078. doi:10.1016/j.rse.2024.114078.
- Yang, M., Mou, Y., Liu, S., Meng, Y., Liu, Z., Li, P., Xiang, W., Zhou, X., Peng, C., 2022. Detecting and mapping tree crowns based on convolutional neural network and Google Earth images. *International Journal of Applied Earth Observation and Geoinformation* 108, 102764. doi:10.1016/j.jag.2022.102764.
- Zeng, W., Tomppo, E., Healey, S.P., Gadow, K.V., 2015. The national forest inventory in China: History - results - international context. *Forest Ecosystems* 2, 23. doi:10.1186/s40663-015-0047-2.
- Zhang, C., Zhou, J., Wang, H., Tan, T., Cui, M., Huang, Z., Wang, P., Zhang, L., 2022. Multi-Species Individual Tree Segmentation and Identification Based on Improved Mask R-CNN and UAV Imagery in Mixed Forests. *Remote Sensing* 14, 874. doi:10.3390/rs14040874.
- Zhang, Y., Ling, F., Wang, X., Foody, G.M., Boyd, D.S., Li, X., Du, Y., Atkinson, P.M., 2021. Tracking small-scale tropical forest disturbances: Fusing the Landsat and Sentinel-2 data record. *Remote Sensing of Environment* 261, 112470. doi:10.1016/j.rse.2021.112470.